iScience

CellPress

Article

SIDT2 RNA Transporter Promotes Lung and Gastrointestinal Tumor Development

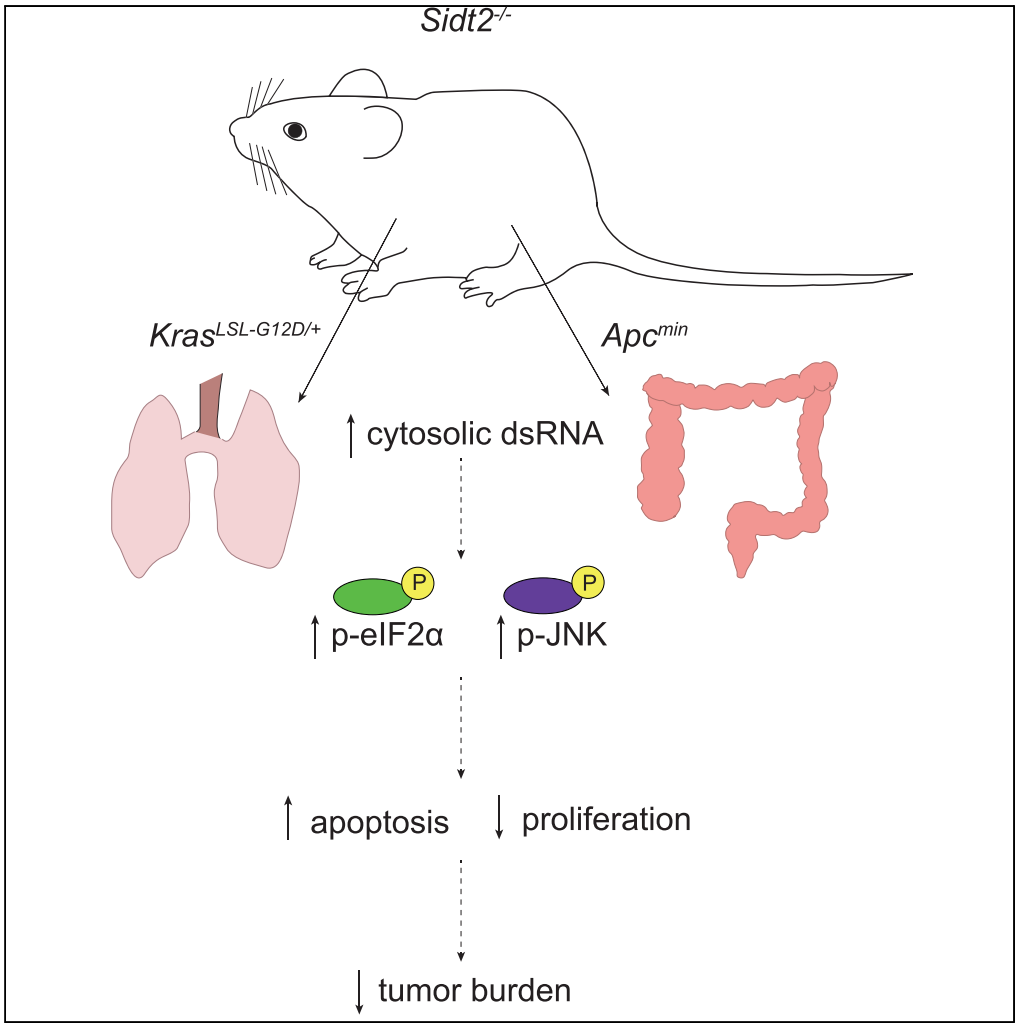

Tan A. Nguyen, Kathryn T. Bieging-Rolett, Tracy L. Putoczki, Ian P. Wicks, Laura D. Attardi, Ken C. Pang

ken.pang@mcri.edu.au

HIGHLIGHTS

Loss of the SIDT2 double-stranded RNA (dsRNA) transporter

leads to accumulation of dsRNA in tissues

is associated with increased apoptosis

reduces tumor burden in mouse models of lung adenocarcinoma and intestinal cancer

Nguyen et al., iScience *20*, 14–24
October 25, 2019
https://doi.org/10.1016/j.isci.2019.09.009

iScience

CellPress

Article

SIDT2 RNA Transporter Promotes Lung and Gastrointestinal Tumor Development

Tan A. Nguyen,[1,2] Kathryn T. Bieging-Rolett,[3,4] Tracy L. Putoczki,[1,2] Ian P. Wicks,[1,2] Laura D. Attardi,[3,4] and Ken C. Pang[1,5,6,7,8,*]

SUMMARY

RNautophagy is a newly described type of selective autophagy whereby cellular RNAs are transported into lysosomes for degradation. This process involves the transmembrane protein SIDT2, which transports double-stranded RNA (dsRNA) across the endolysosomal membrane. We previously demonstrated that SIDT2 is a transcriptional target of *p53*, but its role in tumorigenesis, if any, is unclear. Unexpectedly, we show here that *Sidt2*$^{-/-}$ mice with concurrent oncogenic *Kras*^{G12D} activation develop significantly fewer tumors than littermate controls in a mouse model of lung adenocarcinoma. Consistent with this observation, loss of SIDT2 also leads to enhanced survival and delayed tumor development in an *Apc*$^{min/+}$ mouse model of intestinal cancer. Within the intestine, *Apc*$^{min/+}$;*Sidt2*$^{-/-}$ mice display accumulation of dsRNA in association with increased phosphorylation of eIF2α and JNK as well as elevated rates of apoptosis. Taken together, our data demonstrate a role for SIDT2, and by extension RNautophagy, in promoting tumor development.

INTRODUCTION

The *C. elegans* double-stranded RNA (dsRNA) transporter SID-1 is conserved throughout much of animal evolution, and mammals possess two paralogs, SIDT1 and SIDT2 (Feinberg and Hunter, 2003; Shih and Hunter, 2011). SIDT2 is broadly expressed in mammalian tissue and localizes within late endosomes and lysosomes (Jialin et al., 2010; Nguyen et al., 2017). Human and mouse SIDT2 homologs show 95% sequence identity across the entire protein (832 amino acids) and 100% identity at the C-terminal 100 amino acids (Nguyen et al., 2017). Such a high degree of conservation implies a strongly selected function, and studies have recently emerged that shed light on the role of SIDT2 in mammals.

On the one hand, SIDT2 appears to have retained RNA transporter activity. This was initially suggested by the observation that the ectodomain of SIDT2 binds long dsRNA *in vitro*, similar to *C. elegans* SID-1 (Li et al., 2015). Consistent with this finding, we subsequently discovered that SIDT2 transports viral dsRNA and that this transport is important for anti-viral immunity (Nguyen et al., 2017). More specifically, we found that SIDT2 promotes the trafficking of internalized dsRNA across the endolysosomal membrane and into the cytoplasm, where it is recognized by RNA sensors, which in turn promote anti-viral, type I interferon (IFN) signaling. Loss of SIDT2 thus impairs IFN production and survival after viral infection is significantly reduced (Nguyen et al., 2017). In parallel, SIDT2 has also recently been reported to traffic RNAs *into* the lysosome for degradation in a novel process described as "RNautophagy" (Aizawa et al., 2016). These experiments—performed using cell-free biochemical assays—suggested that SIDT2 promotes destruction of endogenous RNAs by transporting them from the cytosol into the lysosomes. Such transport would thus be in the opposite direction to that described for viral RNAs, but is potentially consistent with previous observations that RNA transport by *C. elegans* SID-1 is bidirectional and dependent on RNA concentration (Shih and Hunter, 2011).

On the other hand, some studies have observed physiological effects of SIDT2 where the relationship to RNA transport, if any, is unclear. For example, mice lacking SIDT2 demonstrate impaired glucose tolerance, decreased serum insulin levels, and defective insulin secretion (Chang et al., 2016; Gao et al., 2013; Yu et al., 2015). Two recent studies also demonstrated that *Sidt2*$^{-/-}$ mice develop non-alcoholic fatty liver disease (Chen et al., 2018; Gao et al., 2016), with one suggesting that this is due to induction of endoplasmic reticulum stress (Gao et al., 2016) and the other proposing that it is the result of defective autophagy (Chen et al., 2018). Finally, work from our group has also demonstrated a potential role for SIDT2 in tumorigenesis (Brady et al., 2011). Specifically, we found that SIDT2 is a transcriptional target of the tumor suppressor p53, that SIDT2 overexpression in *HrasV12;p53*-null mouse embryo fibroblasts impairs cell

[1]The Walter and Eliza Hall Institute of Medical Research, Parkville, VIC, Australia

[2]Department of Medical Biology, University of Melbourne, Parkville, VIC, Australia

[3]Department of Radiation Oncology, Stanford University School of Medicine, Stanford, CA, USA

[4]Department of Genetics, Stanford University School of Medicine, Stanford, CA, USA

[5]Murdoch Children's Research Institute, Parkville, VIC, Australia

[6]Department of Paediatrics, University of Melbourne, Parkville, VIC, Australia

[7]Department of Psychiatry, University of Melbourne, Parkville, VIC, Australia

[8]Lead Contact

*Correspondence: ken.pang@mcri.edu.au

https://doi.org/10.1016/j.isci.2019.09.009

proliferation, and that small hairpin RNA-mediated knockdown of *Sidt2* in a fibrosarcoma model leads to increased tumor growth following transplantation into immunocompromised *Scid* mice (Brady et al., 2011). Together with the observation that *SIDT2* is transcriptionally downregulated in patient tumors compared with healthy tissue (Beck et al., 2017), these findings thus support a possible tumor suppressive role for SIDT2.

In the current study, we further investigated the role of SIDT2 in tumor development. Unexpectedly, we found that mice lacking SIDT2 display reduced tumor burden and increased survival in both lung adenocarcinoma (LUAD) and intestinal cancer models. Moreover, consistent with its role in dsRNA transport, loss of SIDT2 leads to accumulation of dsRNA, resulting in increased phosphorylation of eIF2α and elevated rates of apoptosis. Our findings therefore suggest that SIDT2, and by extension RNautophagy, play a role in promoting tumor development.

RESULTS

Loss of SIDT2 Inhibits Lung Adenocarcinoma Development

Given the finding that *Sidt2* is a p53 target gene, we sought to investigate its role in tumor suppression *in vivo*. Lung cancer is the leading cause of cancer deaths worldwide, and loss or mutation of *p53* is common in this tumor type. Therefore, we examined the role of Sidt2 in LUAD tumorigenesis by employing an autochthonous mouse model in which mice conditionally express oncogenic $Kras^{G12D}$ under the control of a lox-STOP-lox element ($Kras^{LSL\text{-}G12D}$). Intratracheal inoculation of adenoviral Cre recombinase excises the STOP cassette, resulting in expression of $Kras^{G12D}$ specifically in lung cells. $Kras^{G12D}$ expression drives development of non-small-cell lung tumors, and loss of p53 promotes tumor progression in this model (DuPage et al., 2009). To assess the role of SIDT2 in tumorigenesis in this LUAD model, we crossed $Sidt2^{-/-}$ mice previously generated in our laboratory (Nguyen et al., 2017) with $Kras^{LSL\text{-}G12D/+}$ mice and subsequently assessed lung tumor burden in $Kras^{LSL\text{-}G12D/+}$;$Sidt2^{+/+}$ and $Kras^{LSL\text{-}G12D/+}$;$Sidt2^{-/-}$ mice 18 weeks after intratracheal adenoviral inoculation. In contrast to our previous report suggesting that SIDT2 has a tumor suppressive role in fibrosarcoma, light microscopic analysis of H&E-stained lung sections showed that $Sidt2^{-/-}$ animals have reduced tumor burden (Figure 1A). This was confirmed with subsequent quantification, which showed that mice deficient in SIDT2 developed significantly fewer tumors (Figure 1B) and had a significant reduction in overall tumor burden (Figure 1C). Next, we wanted to investigate whether the loss of SIDT2 leads to an impairment of cellular proliferation. To do so, we compared the expression of Ki67, a cellular marker of proliferation, using immunohistochemical staining (Figure 1D). Consistent with an impairment in cellular proliferation, tumors from $Kras^{LSL\text{-}G12D/+}$;$Sidt2^{-/-}$ mice had significantly less Ki67-positive cells compared with controls (Figure 1E). Together, these results thus suggest that SIDT2 facilitates tumor development in the $Kras^{G12D}$ LUAD model.

Loss of SIDT2 Inhibits Growth of Apc^{min} Intestinal Tumors

The difference in the role for SIDT2 in tumorigenesis in the mouse fibrosarcoma and LUAD models prompted us to test another mouse tumor model to examine for context dependency of Sidt2 in cancer. To this end, we chose the well characterized Apc^{min} mouse model of intestinal cancer. These mice harbor a dominant mutation in the oncogenic *Apc* gene, which leads to spontaneous development of adenomatous polyps, primarily in the distal small intestine (DSI) (Moser et al., 1990; Su et al., 1992).

We subsequently generated $Apc^{min/+}$ mice lacking *Sidt2* (Figure S1) and monitored the animals over time, sacrificing them after the onset of anemia and/or signs of ill health associated with death in this model (e.g., hunching of the back, weight loss). $Apc^{min/+}$;$Sidt2^{-/-}$ mice (median survival: 131 days) survived significantly longer than both $Apc^{min/+}$;$Sidt2^{+/+}$ and $Apc^{min/+}$;$Sidt2^{+/-}$ mice (median survival: 93 and 99 days, respectively), suggesting that loss of SIDT2 impairs intestinal tumor development (Figure 2A). To investigate further, $Apc^{min/+}$;$Sidt2^{-/-}$ mice were sacrificed at day 100 and appeared to have a lower tumor burden within the DSI compared with $Apc^{min/+}$;$Sidt2^{+/+}$ mice (Figure 2B). To properly assess this, tumor number (Figures 2C–2E) and tumor area (Figures 2F–2H) were calculated in the DSI, medial small intestine (MSI), and proximal small intestine (PSI) of 100-day-old $Apc^{min/+}$;$Sidt2^{+/+}$ and $Apc^{min/+}$;$Sidt2^{-/-}$ mice. There was no difference in tumor number in the colon (Figure S2A) or PSI, whereas $Apc^{min/+}$;$Sidt2^{-/-}$ mice had significantly fewer tumors than $Apc^{min/+}$;$Sidt2^{+/+}$ mice in the MSI and DSI. Moreover, $Apc^{min/+}$;$Sidt2^{-/-}$ mice also had smaller tumors than $Apc^{min/+}$;$Sidt2^{+/+}$ mice in the DSI, MSI, and PSI, but again showed no difference in the colon, where tumors are uncommon (Figure S2B). Together, these results suggest that SIDT2 also facilitates tumor development in the Apc^{min} mouse model of intestinal cancer.

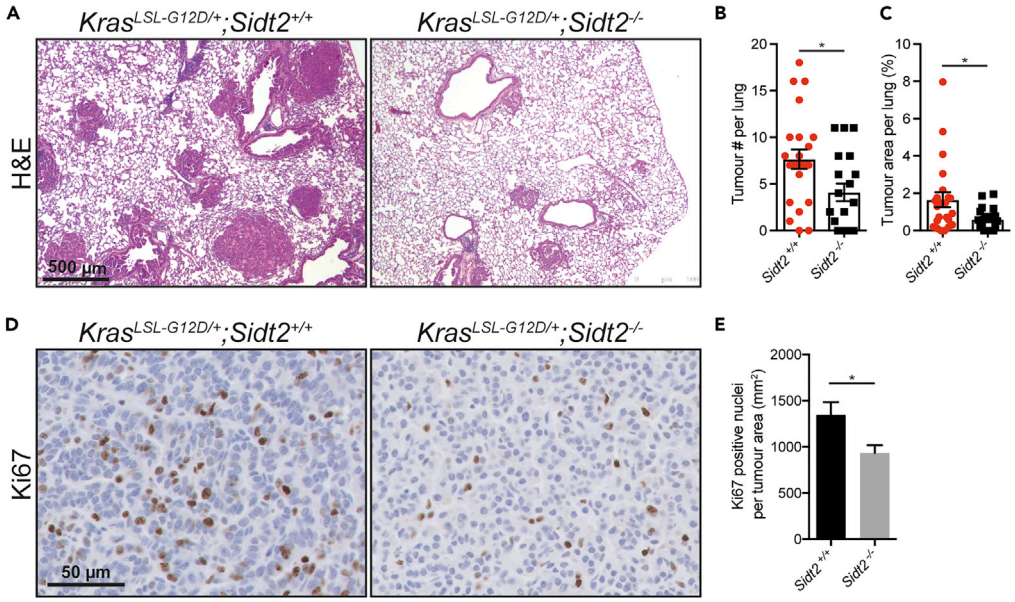

Figure 1. *Kras*$^{LSL\text{-}G12D/+}$;*Sidt2*$^{-/-}$ Mice Have Increased Tumor Burden Compared with Controls

(A) Representative images of H&E-stained lung sections from *Kras*$^{LSL\text{-}G12D/+}$;*Sidt2*$^{+/+}$ and *Kras*$^{LSL\text{-}G12D/+}$;*Sidt2*$^{-/-}$ mice 18 weeks following inoculation with 4 × 10^6 plaque-forming unit adenovirus containing Cre recombinase by intratracheal intubation.

(B and C) (B) Average tumor number and (C) tumor burden as a percentage of total lung area was assessed per lung section (n = 19–23 mice per genotype).

(D) Representative images of Ki67-stained lung sections of *Kras*$^{LSL\text{-}G12D/+}$;*Sidt2*$^{+/+}$ and *Kras*$^{LSL\text{-}G12D/+}$;*Sidt2*$^{-/-}$ mice.

(E) Quantification of average number of Ki67-positive cells per mm^2 tumor tissue. Analysis was performed on >25 tumors per mouse (n = mice per genotype).

Error bars represent ±SEM. *p < 0.05, as calculated by unpaired Student's t test.

As *Apc*$^{min/+}$;*Sidt2*$^{-/-}$ mice had significantly smaller tumors than *Apc*$^{min/+}$;*Sidt2*$^{+/+}$ mice across all segments of the small intestine (Figures 2G–2I), we hypothesized that loss of SIDT2 does not affect tumor initiation, but instead plays a role in the growth of tumors by impairing cell proliferation. To investigate this possibility, we compared the expression of Ki67 in tumors of *Apc*$^{min/+}$;*Sidt2*$^{-/-}$ and *Apc*$^{min/+}$;*Sidt2*$^{+/+}$ mice (Figure 3A). Consistent with the decrease in Ki67-positive cells observed in *Kras*$^{LSL\text{-}G12D/+}$;*Sidt2*$^{-/-}$ mice, *Apc*$^{min/+}$;*Sidt2*$^{-/-}$ mice had significantly less Ki67-positive staining overall (Figure 3B), as well as fewer intratumoral Ki67-positive cells (Figure 3C) compared with *Apc*$^{min/+}$;*Sidt2*$^{+/+}$ mice.

SIDT2 Is Required to Prevent dsRNA Accumulation and PKR/eIF2α Pathway Activation

Given the role of SIDT2 in transporting dsRNA across the endolysosomal membrane (Nguyen et al., 2017), we next assessed the effect of SIDT2 on the subcellular localization of dsRNA within the DSI. To do so, we performed immunofluorescence staining on frozen sections of the DSI of 100-day-old *Apc*$^{min/+}$;*Sidt2*$^{-/-}$ and *Apc*$^{min/+}$;*Sidt2*$^{+/+}$ mice using the J2 monoclonal antibody (Figure 4A), which specifically detects dsRNA helices at least 40 bp in length, in a sequence-independent manner (Schonborn et al., 1991). Notably, staining for dsRNA was readily observed within the intestinal crypts of *Apc*$^{min/+}$;*Sidt2*$^{-/-}$ mice but was absent in crypts of *Apc*$^{min/+}$;*Sidt2*$^{+/+}$ animals and in other parts of the DSI, including tumors (Figure 4B). To confirm that this was not specific to the *Apc*$^{min/+}$ mouse model, we also performed dsRNA staining in lungs of *Kras*$^{LSL\text{-}G12D/+}$; *Sidt2*$^{+/+}$ and *Kras*$^{LSL\text{-}G12D/+}$; *Sidt2*$^{-/-}$ mice using immunohistochemistry (Figure S3A). Consistent with our previous data, we observed a significant increase in cytosolic dsRNA staining in *Kras*$^{LSL\text{-}G12D/+}$; *Sidt2*$^{-/-}$ mice compared with controls (Figure S3B), suggesting that loss of SIDT2 leads to accumulation of dsRNA in the cytosol.

Cytosolic dsRNAs are bound by RNA-dependent protein kinase (PKR), leading to its autophosphorylation and activation (Garcia et al., 2006). Activated PKR subsequently phosphorylates the α subunit of protein synthesis initiation factor eIF2 (eIF2α), resulting in inhibition of protein translation as well as anti-viral

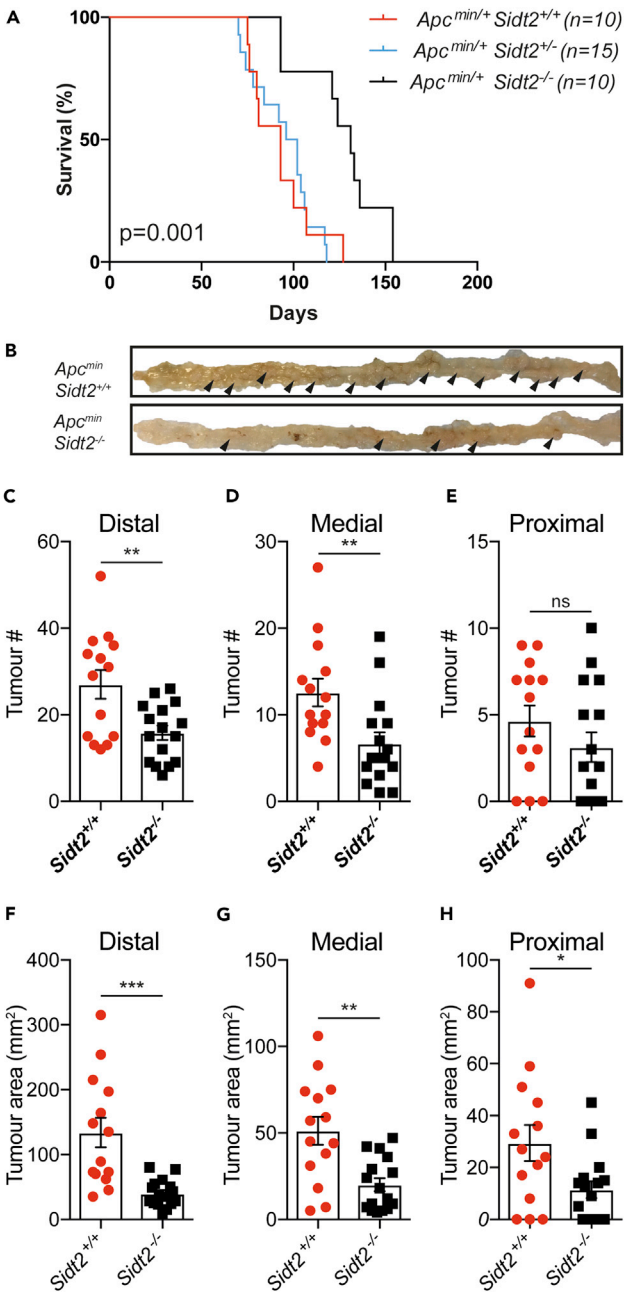

Figure 2. - *Apc*$^{min/+}$;*Sidt2*$^{-/-}$ Mice Have Enhanced Survival and Smaller Tumors Compared with Controls

(A) Kaplan-Meier survival curve of *Apc*$^{min/+}$;*Sidt2*$^{+/+}$, *Apc*$^{min/+}$;*Sidt2*$^{+/-}$, and *Apc*$^{min/+}$;*Sidt2*$^{-/-}$ mice. Median survival rates of *Apc*$^{min/+}$;*Sidt2*$^{+/+}$, *Apc*$^{min/+}$;*Sidt2*$^{+/-}$, and *Apc*$^{min/+}$;*Sidt2*$^{-/-}$ mice are 93, 99, and 131 days respectively.

(B–I) (B) Representative image of distal small intestine of 100-day-old *Apc*$^{min/+}$;*Sidt2*$^{+/+}$ and *Apc*$^{min/+}$;*Sidt2*$^{-/-}$ mouse. Total number (C–E) and area (F–H) of visible tumors in the colon and small intestine (distal, medial, and proximal) was quantified in 100-day-old *Apc*$^{min/+}$;*Sidt2*$^{+/+}$ (n = 12) and *Apc*$^{min/+}$;*Sidt2*$^{-/-}$ (n = 12) mice.

Error bars represent mean ± SEM. *p < 0.05, **p < 0.01, ***p < 0.001 as calculated by unpaired Student's t test.

See also Figures S1 and S2.

and anti-tumor effects (Gao et al., 2013; Gao et al., 2016). We therefore wished to determine whether the accumulation of dsRNA in cells deficient in SIDT2 was likely to activate PKR. Although we tested multiple antibodies raised against phosphorylated PKR, none showed an ability to recognize activated murine PKR in control samples via western blot (data not shown), so instead we compared phosphorylation of eIF2α as a

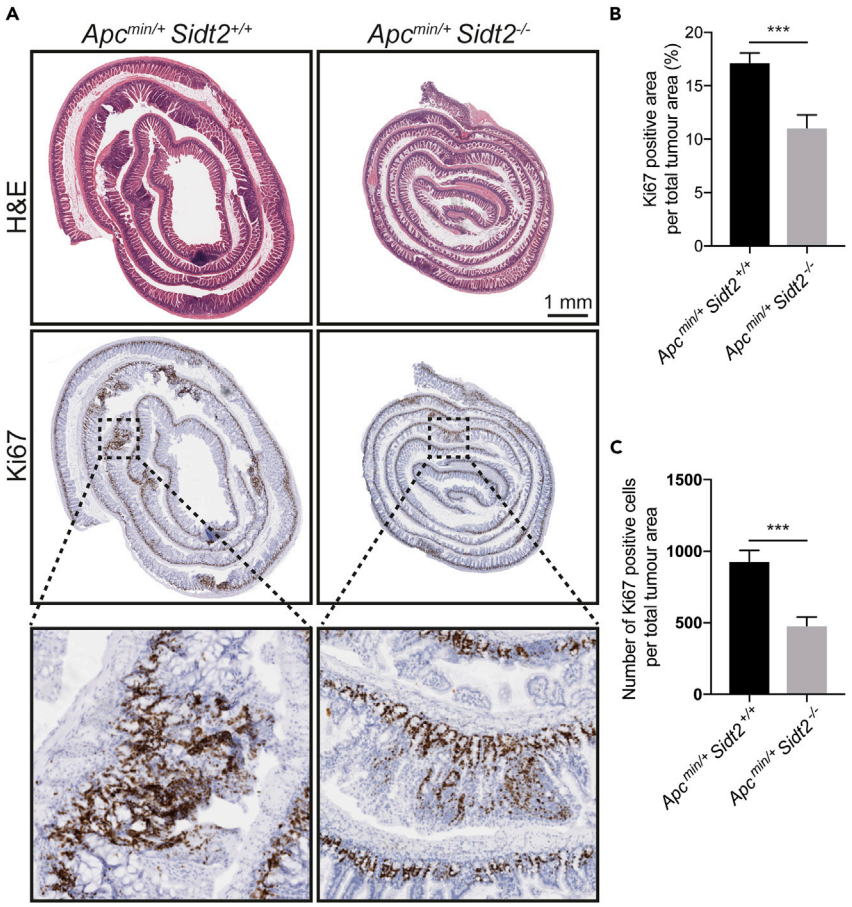

Figure 3. Loss of SIDT2 Impairs Tumor Proliferation

(A–C) (A) Representative H&E- and Ki67-stained histological sections of distal small intestine of $Apc^{min/+}$;$Sidt2^{+/+}$ and $Apc^{min/+}$;$Sidt2^{-/-}$ mice at 100 days of age. Quantification of (B) Ki67-positive staining area as a percentage of total tumor area and (C) average number of Ki67-positive cells per tumor. Analysis was performed on >20 high-power fields across three mice. Error bars represent mean ± SEM. ***p < 0.001 as calculated by unpaired Student's t test.

proxy for PKR activation. Moreover, because we only observed SIDT2-dependent dsRNA accumulation in the intestinal crypts and not in tumors themselves, we analyzed p-eIF2α expression separately in non-tumor and tumor tissues from the DSI of $Apc^{min/+}$;$Sidt2^{-/-}$ and $Apc^{min/+}$;$Sidt2^{+/+}$ mice. Notably, $Apc^{min/+}$;$Sidt2^{+/+}$ mice displayed higher p-eIF2α levels in non-tumor tissue (Figure 4C), consistent with dsRNA accumulation and activation of PKR within these cells. This SIDT2-dependent increase in p-eIF2α was less apparent in tumor tissue (Figure 4D).

In addition to its role in the inhibition of protein translation, PKR activation has been shown to mediate cellular stress responses via regulation of mitogen-activated protein kinases such as c-Jun n-terminal kinase (JNK) (Goh et al., 2000; Kim et al., 2014; Taghavi and Samuel, 2012) and promote apoptosis via caspase 8 and nuclear factor-κB (Gil and Esteban, 2000). In line with our hypothesis that PKR activation is increased in the intestinal crypts in the absence of SIDT2, we observed a concurrent increase in phosphorylation of JNK in normal intestinal tissue of $Apc^{min/+}$;$Sidt2^{-/-}$ mice compared with $Apc^{min/+}$;$Sidt2^{+/+}$ mice (Figures 5A and 5B). To assess whether loss of SIDT2 leads to increased caspase 8-mediated apoptosis, we assessed and compared cleavage of caspase 8 in the DSI of $Apc^{min/+}$;$Sidt2^{-/-}$ and $Apc^{min/+}$;$Sidt2^{+/+}$ mice and observed an increase in caspase 8 cleavage products in $Apc^{min/+}$;$Sidt2^{-/-}$ normal intestinal tissue (Figures 5A and 5C). We next performed immunohistochemical staining on intestinal Swiss rolls of $Apc^{min/+}$;$Sidt2^{-/-}$ and $Apc^{min/+}$;$Sidt2^{+/+}$ mice (Figure 5D), which revealed an increased number of cleaved-caspase 3-positive cells within intestinal crypts lacking SIDT2 (Figure 5E). This was further confirmed via TUNEL staining in which $Apc^{min/+}$;$Sidt2^{-/-}$ showed increased TUNEL-positive cells within

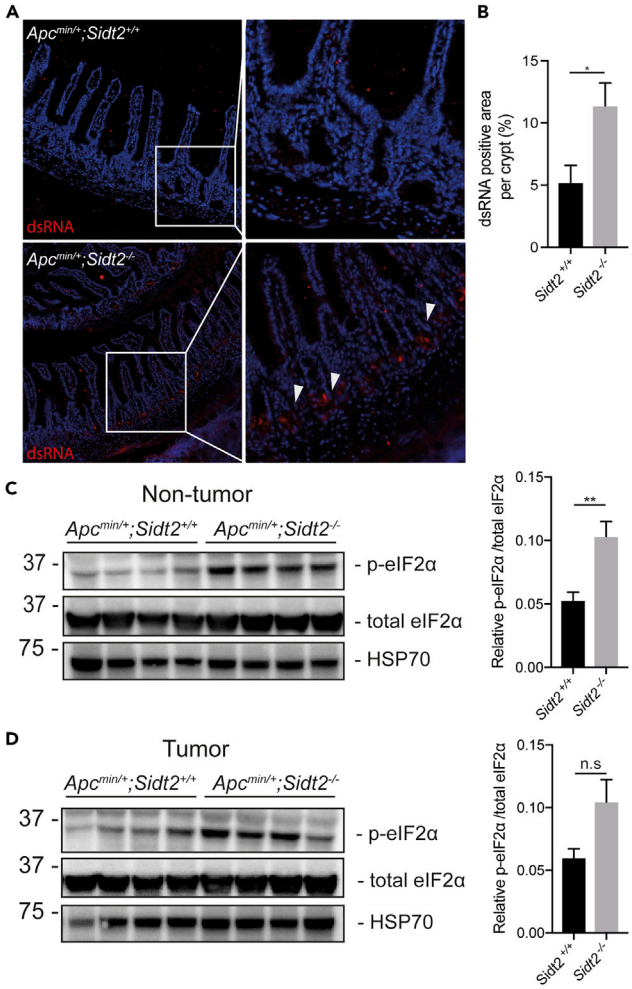

Figure 4. - Loss of SIDT2 Leads to dsRNA Accumulation within Intestinal Crypts and Increased Phosphorylation of eIF2α

(A) Representative image of dsRNA staining of distal small intestine of 100-day-old *Sidt2*$^{+/+}$;*Apc*$^{min/+}$ and *Sidt2*$^{-/-}$;*Apc*$^{min/+}$ mice. Arrowheads indicate cells with positive dsRNA staining.

(B–D) (B) Quantification of dsRNA-positive stained area per crypt (n = 3–4 mice per genotype). Western blot and densitometry analysis of eIF2α phosphorylation in non-tumor (C) and tumor (D) tissue from distal small intestine of 100-day-old *Sidt2*$^{+/+}$;*Apc*$^{min/+}$ and *Sidt2*$^{-/-}$;*Apc*$^{min/+}$ mice normalized to total eIF2α. Each lane corresponds to an individual mouse (n = 4 mice per genotype). Error bars represent mean ± SEM. *p < 0.05, **p < 0.01 as calculated by unpaired Student's t test.

See also Figures S3 and S4.

intestinal crypts compared with controls (Figure 5F). Taken together, these data strongly imply that loss of SIDT2 leads to increased caspase 8- and caspase 3-mediated apoptosis within intestinal crypts, consistent with the restricted tumor growth observed in *Apc*$^{min/+}$;*Sidt2*$^{-/-}$ animals.

Lower *SIDT2* Expression Is Associated with Improved Survival in Different Human Cancers

Finally, to explore the role of SIDT2 in human cancer, we determined whether different levels of intratumoral *SIDT2* expression are associated with changes in patient survival. Using data collected by The Cancer Genome Atlas Research Network (http://cancergenome.nih.gov/) and analyzed via The Pathology Atlas (Uhlen et al., 2017), we observed that lower intratumoral *SIDT2* RNA levels were associated with significantly improved prognosis in 5 of 17 different cancers (renal, thyroid, gastric, glioma, urothelial) (Figures 6A–6E). However, consistent with a context-dependent role, intratumoral *SIDT2* RNA levels showed no prognostic significance in 10 other cancers (including LUAD and colon cancer), and lower

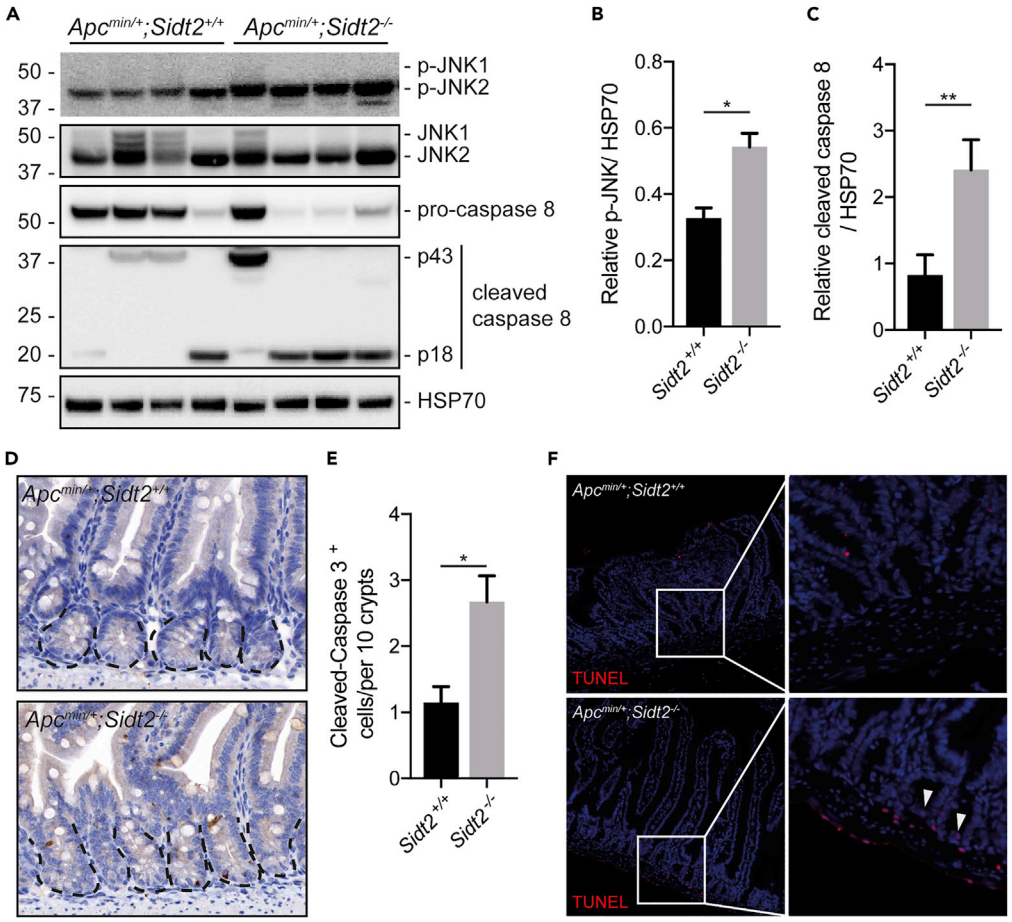

Figure 5. - *Sidt2*$^{-/-}$;*Apc*$^{min/+}$ Mice Have Increased Apoptosis in Intestinal Tissue

(A–C) (A) Western blot analysis. Phosphorylation of JNK and cleavage of caspase 8 was assessed in normal intestinal tissue of 100-day-old *Sidt2*$^{+/+}$;*Apc*$^{min/+}$ and *Sidt2*$^{-/-}$;*Apc*$^{min/+}$ mice. Each lane corresponds to an individual mouse (n = 4 mice per genotype). Densitometry quantification of (B) p-JNK and (C) cleaved caspase 8 normalized to HSP70.

(D) Representative images of cleaved caspase 3 staining of distal small intestine of 100-day-old *Sidt2*$^{+/+}$;*Apc*$^{min/+}$ and *Sidt2*$^{-/-}$;*Apc*$^{min/+}$ mice.

(E) Quantification of dsRNA-positive stained area per crypt (n = 7 mice per genotype).

(F) Representative images of TUNEL staining of positive cells from distal small intestine of 100-day-old *Sidt2*$^{+/+}$;*Apc*$^{min/+}$ and *Sidt2*$^{-/-}$;*Apc*$^{min/+}$ mice, n = 3 animals per genotype. Arrowheads indicate TUNEL^{+} cells.

Error bars represent mean ± SEM. *$p < 0.05$, **$p < 0.01$ as calculated by unpaired Student's t test.

See also Figure S4.

intratumoral *SIDT2* levels were actually associated with poorer survival in pancreatic and cervical cancers (Figure S5).

DISCUSSION

In this study, we show that the mammalian SID-1 ortholog SIDT2, which is a transcriptional target for p53, promotes tumor growth. Specifically, loss of SIDT2 in mice caused reduced tumor burden and enhanced survival, with the latter observation supported by data from patients with several different cancers in which lower *SIDT2* expression was associated with an improved prognosis.

Mechanistically, our data from *Apc*^{min} animals suggest a model in which the absence of SIDT2 leads to impaired RNautophagy, accumulation of intracellular dsRNA, increased phosphorylation of eIF2α and JNK, and finally, increased apoptosis via activation of caspase 8 (Figure 7). Notably, when visualized, these changes were only observed in the intestinal crypts and not in tumors themselves, and is potentially in

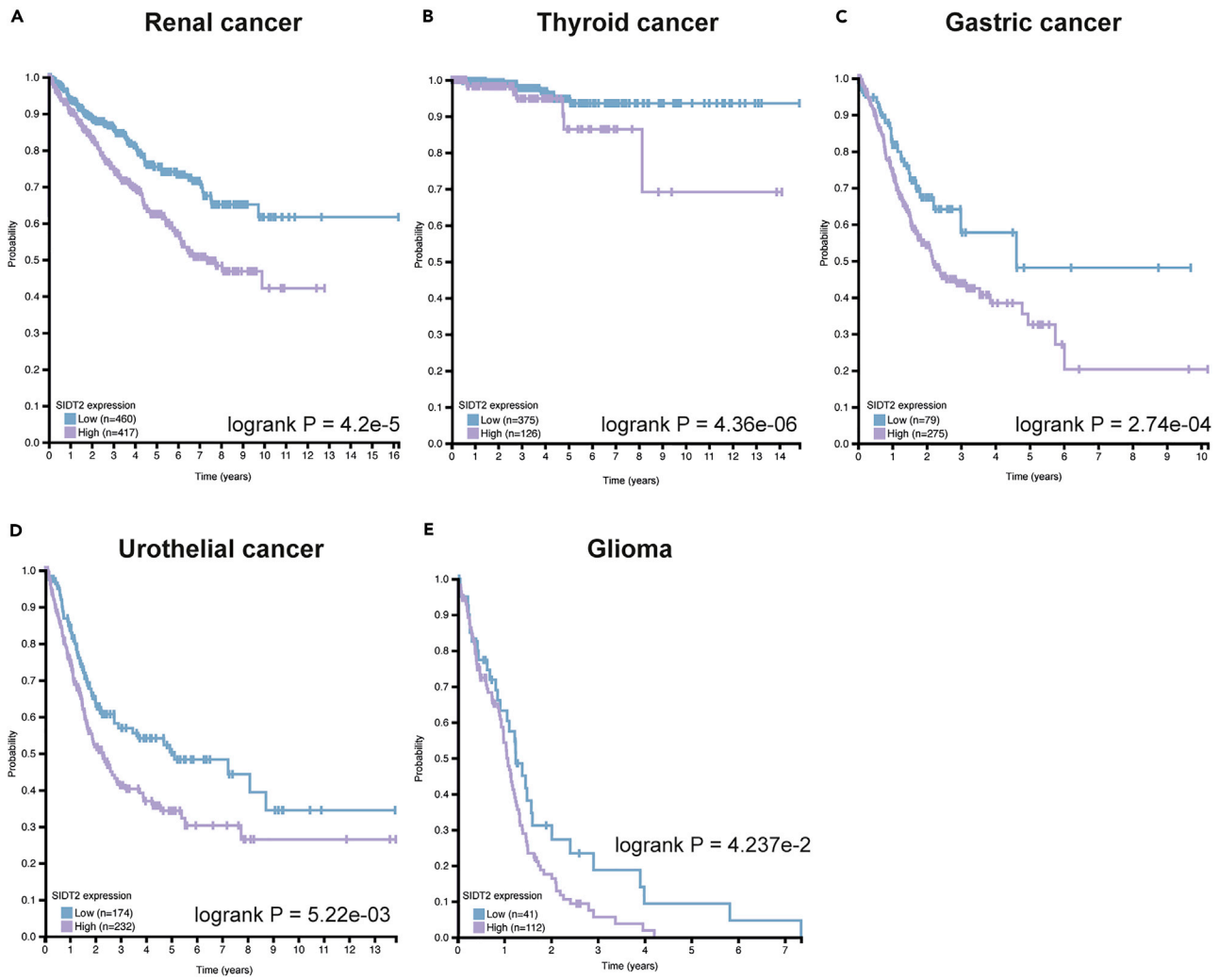

Figure 6. – Lower SIDT2 Expression Is Associated with Improved Survival in Some Cancers

(A–E) Kaplan-Meier curves of overall survival of patients with (A) renal, (B) thyroid, (C) gastric, and (D) urothelial cancer and (E) glioma stratified against *SIDT2* expression from publicly available RNA-seq data. The results shown are in whole based upon data generated by the TCGA Research Network: http://cancergenome.nih.gov/.

See also Figure S5.

keeping with the strong expression of SIDT2 observed within the crypts of human small intestine (Uhlen et al., 2017) (Figure S4). Nevertheless, such observations invite the question of how such crypt-related changes could impact subsequent tumor growth. One possible explanation is that the increased apoptosis observed in SIDT2-deficient mice affects cancer stem cells, which reside within the intestinal crypt and play a key role in subsequent tumor growth. Consistent with this, selective depletion of intestinal stem cells has previously been shown to restrict primary tumor growth in mice (de Sousa e Melo et al., 2017), and this would be in keeping with our observation that SIDT2-deficient tumors show reduced proliferation (Figure 3). Another possible explanation is that increased eIF2α activation in the absence of SIDT2 induces differentiation (and thus loss) of these same intestinal stem cells, as has been observed by others (Heijmans et al., 2013). Further work to investigate the specific effects of SIDT2 on cancer stem cell development will hopefully shed light on these possibilities.

Notwithstanding our inability to activate PKR (see below), PKR seems a likely candidate in mediating the downstream effects in our Apc^{min} $Sidt2^{-/-}$ mice. After all, PKR has well-established roles not only in binding and responding to intracellular dsRNA but also in inducing eIF2α phosphorylation, JNK activation, and caspase 8-mediated activation of caspase 3 to induce apoptosis. Consistent with our results, PKR expression

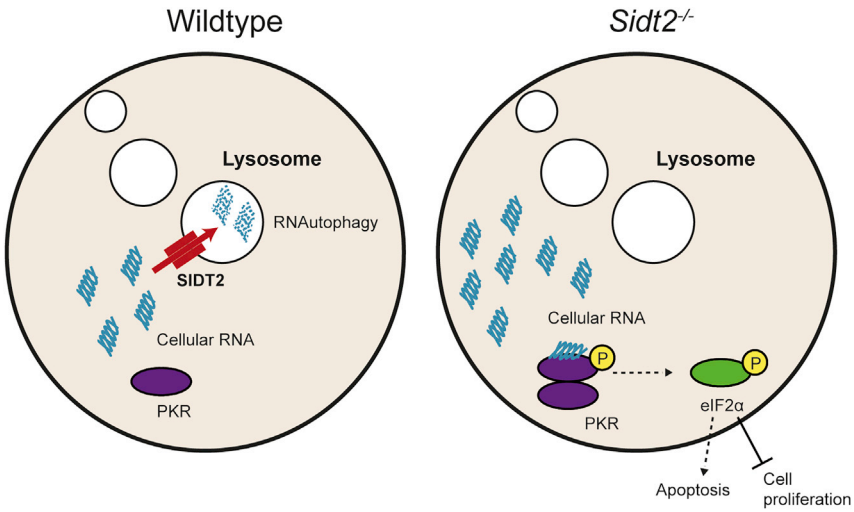

Figure 7. Loss of SIDT2-Mediated RNAutophagy Leads to Increased Apoptosis and Cell Proliferation

SIDT2 is a dsRNA transporter that mediates the lysosomal degradation of cellular RNAs via RNAutophagy. Loss of SIDT2 leads to accumulation of cellular RNA within the cytosol. Binding of these RNAs by protein kinase RNA-activated (PKR) leads to its activation and subsequent phosphorylation of eukaryotic translation initiation factor 2 alpha (eIF2α). Phosphorylation of eIF2α leads to inhibition of protein translation and cell proliferation, as well as induction of apoptosis.

and auto-phosphorylation have previously been reported to be increased in multiple human malignancies, including colon and lung cancer (Kim et al., 2000, 2002), and those with higher p-PKR and p-eIF2α had significantly longer survival (Guo et al., 2013; He et al., 2011; Pataer et al., 2010).

Given the presence of intracellular dsRNA in Apc^{min};$Sidt2^{-/-}$ intestinal crypts, we also assessed whether there was induction of a type I IFN response in these tissues. However, we were unable to detect upregulation of *Ifnβ* or various IFN-stimulated genes in tissues of $Apc^{min/+}$;$Sidt2^{-/-}$ mice (data not shown), suggesting that the reduced tumor burden observed in SIDT2-deficient mice is unlikely to be due to the anti-tumor effects of type I IFN (Dunn et al., 2006). This lack of a type I IFN response may also provide a clue as to the nature of the dsRNA that accumulates in the absence of SIDT2. Specifically, the type I IFN response to cytoplasmic dsRNA is mainly orchestrated by the RIG-I-like receptors, RIG-I and MDA-5 (Laessig and Hopfner, 2017; Yoneyama and Fujita, 2010). RIG-I specifically recognizes short dsRNA and ssRNA with 5′ triphosphate ends (Hornung et al., 2006), a common feature of viral RNAs, and MDA-5 is critical for the detection of long dsRNAs (>1,000 bp) (Kato et al., 2006; Peisley et al., 2012, 2011). The lack of a detectable type I IFN response in $Apc^{min/+}$;$Sidt2^{-/-}$ mice therefore suggests that the dsRNAs that accumulate in the intestinal crypts of these animals do not possess 5′triphosphate ends and are not long enough to activate MDA-5. In contrast, PKR requires a minimum dsRNA region of only 30 bp (Lemaire et al., 2008; Manche et al., 1992) and can recognize RNAs with limited stem loop or duplex structures (Osman et al., 1999), including small interfering RNA (Puthenveetil et al., 2006; Sledz et al., 2003), small nucleolar RNA (Youssef et al., 2015), and bacterial RNAs (Hull and Bevilacqua, 2015). Indeed, PKR has recently been reported to bind endogenous nuclear dsRNAs during cell mitosis (Kim et al., 2014), noncoding Alu RNA and mitochondrial RNAs that are capable of forming intramolecular dsRNA structures (Kim et al., 2018). These RNA species may therefore be more likely to accumulate in the absence of SIDT2. At the same time, it has been proposed that autophagy is important for the degradation of many types of cytosolic RNAs, including retrotransposon, viral, and cellular messenger RNAs (Aizawa et al., 2016; Guo et al., 2014; Orvedahl et al., 2010), so impaired lysosomal degradation of RNA in the absence of SIDT2 could also lead to accumulation of these RNAs within the intestinal crypt. Future studies to identify the RNA cargo of SIDT2 within the intestine will clarify these possibilities.

Finally, it should be noted that the apparent protective effect of lower intratumoral *SIDT2* levels on patient survival was limited to certain types of cancers. Moreover, in pancreatic and cervical cancers, lower intratumoral *SIDT2* levels were associated with poorer survival. Thus, the role of SIDT2 in promoting tumor growth may only apply in specific contexts, and this may explain the apparent contradiction between the data described here and our earlier findings, namely, that SIDT2 functions as a tumor suppressor in a

fibrosarcoma model (Brady et al., 2011). Regardless, the results from this study identify a role for SIDT2 and RNautophagy in promoting cancer development *in vivo* and suggest the possibility that strategies to inhibit SIDT2 and/or RNautophagy could be a useful adjunct to existing treatment for certain types of cancer.

Limitations of Study

In this study, we were unable to directly show that the accumulation of dsRNA in *Sidt2*$^{-/-}$ mice leads to increased PKR activation. This was despite trying a range of different approaches, including commercial antibodies designed to detect phosphorylated murine PKR, phos-tag gels, and direct mass spectrometry methods. Reliable detection of murine phospho-PKR is a problem that is well recognized in the field, and future studies using *Sidt2*$^{-/-}$;*Pkr*$^{-/-}$ animals may shed further light on the mechanistic interplay between these two proteins in cancer development.

METHODS

All methods can be found in the accompanying Transparent Methods supplemental file.

SUPPLEMENTAL INFORMATION

Supplemental Information can be found online at https://doi.org/10.1016/j.isci.2019.09.009.

ACKNOWLEDGMENTS

We thank R. Crawley, S. Russo, C. Hay, and L. Wilkins for technical assistance. We also thank S. Davidson and B. Feltham as well all members of the Masters, Putoczki, and Wicks laboratories for helpful discussions and gifts of reagents. This work was supported by the Australian NHMRC (ID 1064591), Royal Australasian College of Physicians, Reid Family Trust, Lung Foundation Australia, and Cancer Council Victoria. NIH grant R35 CA197591 to L.D.A.

AUTHOR CONTRIBUTIONS

K.C.P., T.A.N., K.T.B.-R., T.L.P., I.P.W., and L.D.A. designed experiments and/or analyzed the data. T.A.N. and K.T.B.-R. performed experiments. K.C.P. and T.A.N. wrote the manuscript. K.C.P., L.D.A., and I.P.W. supervised the project.

DECLARATION OF INTERESTS

The authors declare no competing interests.

Received: July 6, 2018
Revised: August 20, 2019
Accepted: September 5, 2019
Published: October 25, 2019

REFERENCES

Aizawa, S., Fujiwara, Y., Contu, V.R., Hase, K., Takahashi, M., Kikuchi, H., Kabuta, C., Wada, K., and Kabuta, T. (2016). Lysosomal putative RNA transporter SIDT2 mediates direct uptake of RNA by lysosomes. Autophagy *12*, 565–578.

Beck, A., Fecher-Trost, C., Wolske, K., Philipp, S.E., Flockerzi, V., and Wissenbach, U. (2017). Identification of Sidt2 as a lysosomal cation-conducting protein. FEBS Lett. *591*, 76–87.

Brady, C.A., Jiang, D., Mello, S.S., Johnson, T.M., Jarvis, L.A., Kozak, M.M., Kenzelmann Broz, D., Basak, S., Park, E.J., McLaughlin, M.E., et al. (2011). Distinct p53 transcriptional programs dictate acute DNA-damage responses and tumor suppression. Cell *145*, 571–583.

Chang, G., Yang, R., Cao, Y., Nie, A., Gu, X., and Zhang, H. (2016). Sidt2 is involved in the NAADP-mediated release of calcium from insulin secretory granules. J. Mol. Endocrinol. *56*, 249–259.

Chen, X., Gu, X., and Zhang, H. (2018). Sidt2 regulates hepatocellular lipid metabolism through autophagy. J. Lipid Res. *59*, 404–415.

de Sousa e Melo, F., Kurtova, A.V., Harnoss, J.M., Kljavin, N., Hoeck, J.D., Hung, J., Anderson, J.E., Storm, E.E., Modrusan, Z., Koeppen, H., et al. (2017). A distinct role for Lgr5+ stem cells in primary and metastatic colon cancer. Nature *543*, 676–680.

Dunn, G.P., Koebel, C.M., and Schreiber, R.D. (2006). Interferons, immunity and cancer immunoediting. Nat. Rev. Immunol. *6*, 836–848.

DuPage, M., Dooley, A.L., and Jacks, T. (2009). Conditional mouse lung cancer models using adenoviral or lentiviral delivery of Cre recombinase. Nat. Protoc. *4*, 1064–1072.

Feinberg, E.H., and Hunter, C.P. (2003). Transport of dsRNA into cells by the transmembrane protein SID-1. Science *301*, 1545–1547.

Gao, J., Gu, X., Mahuran, D.J., Wang, Z., and Zhang, H. (2013). Impaired glucose tolerance in a mouse model of sidt2 deficiency. PLoS One *8*, e66139.

Gao, J., Zhang, Y., Yu, C., Tan, F., and Wang, L. (2016). Spontaneous nonalcoholic fatty liver disease and ER stress in Sidt2 deficiency mice. Biochem. Biophys. Res. Commun. *476*, 326–332.

Garcia, M.A., Gil, J., Ventoso, I., Guerra, S., Domingo, E., Rivas, C., and Esteban, M. (2006). Impact of protein kinase PKR in cell biology: from

antiviral to antiproliferative action. Microbiol. Mol. Biol. Rev. *70*, 1032–1060.

Gil, J., and Esteban, M. (2000). Induction of apoptosis by the dsRNA-dependent protein kinase (PKR): mechanism of action. Apoptosis *5*, 107–114.

Goh, K.C., deVeer, M.J., and Williams, B.R. (2000). The protein kinase PKR is required for p38 MAPK activation and the innate immune response to bacterial endotoxin. EMBO J. *19*, 4292–4297.

Guo, C., Shao, R., Correa, A.M., Behrens, C., Johnson, F.M., Raso, M.G., Prudkin, L., Solis, L.M., Nunez, M.I., Fang, B., et al. (2013). Prognostic significance of combinations of RNA-dependent protein kinase and EphA2 biomarkers for NSCLC. J. Thorac. Oncol. *8*, 301–308.

Guo, H., Chitiprolu, M., Gagnon, D., Meng, L., Perez-Iratxeta, C., Lagace, D., and Gibbings, D. (2014). Autophagy supports genomic stability by degrading retrotransposon RNA. Nat. Commun. *5*, 5276.

He, Y., Correa, A.M., Raso, M.G., Hofstetter, W.L., Fang, B., Behrens, C., Roth, J.A., Zhou, Y., Yu, L., Wistuba, I.I., et al. (2011). The role of PKR/eIF2α signaling pathway in prognosis of non-small cell lung cancer. PLoS One *6*, e24855.

Heijmans, J., van Lidth de Jeude, J.F., Koo, B.-K., Rosekrans, S.L., Wielenga, M.C.B., van de Wetering, M., Ferrante, M., Lee, A.S., Onderwater, J.J.M., Paton, J.C., et al. (2013). ER stress causes rapid loss of intestinal epithelial stemness through activation of the unfolded protein response. Cell Rep. *3*, 1128–1139.

Hornung, V., Ellegast, J., Kim, S., Brzózka, K., Jung, A., Kato, H., Poeck, H., Akira, S., Conzelmann, K.-K., Schlee, M., et al. (2006). 5′-Triphosphate RNA is the ligand for RIG-I. Science *314*, 994–997.

Hull, C.M., and Bevilacqua, P.C. (2015). Mechanistic analysis of activation of the innate immune sensor PKR by bacterial RNA. J. Mol. Biol. *427*, 3501–3515.

Jialin, G., Xuefan, G., and Huiwen, Z. (2010). SID1 transmembrane family, member 2 (Sidt2): a novel lysosomal membrane protein. Biochem. Biophys. Res. Commun. *402*, 588–594.

Kato, H., Takeuchi, O., Sato, S., Yoneyama, M., Yamamoto, M., Matsui, K., Uematsu, S., Jung, A., Kawai, T., Ishii, K.J., et al. (2006). Differential roles of MDA5 and RIG-I helicases in the recognition of RNA viruses. Nature *441*, 101–105.

Kim, S.H., Forman, A.P., Mathews, M.B., and Gunnery, S. (2000). Human breast cancer cells contain elevated levels and activity of the protein kinase, PKR. Oncogene *19*, 3086–3094.

Kim, S.H., Gunnery, S., Choe, J.K., and Mathews, M.B. (2002). Neoplastic progression in melanoma and colon cancer is associated with increased expression and activity of the interferon-inducible protein kinase, PKR. Oncogene *21*, 8741–8748.

Kim, Y., Lee, J.H., Park, J.-E., Cho, J., Yi, H., and Kim, V.N. (2014). PKR is activated by cellular dsRNAs during mitosis and acts as a mitotic regulator. Genes Dev. *28*, 1310–1322.

Kim, Y., Park, J., Kim, S., Kim, M., Kang, M.-G., Kwak, C., Kang, M., Kim, B., Rhee, H.-W., and Kim, V.N. (2018). PKR senses nuclear and mitochondrial signals by interacting with endogenous double-stranded RNAs. Mol. Cell *71*, 1051–1063.e6.

Laessig, C., and Hopfner, K.-P. (2017). Discrimination of cytosolic self and non-self RNA by RIG-I-like receptors. J. Biol. Chem. *292*, 9000–9009.

Lemaire, P.A., Anderson, E., Lary, J., and Cole, J.L. (2008). Mechanism of PKR activation by dsRNA. J. Mol. Biol. *381*, 351–360.

Li, W., Koutmou, K.S., Leahy, D.J., and Li, M. (2015). Systemic RNA interference deficiency-1 (SID-1) extracellular domain selectively binds long double-stranded RNA and is required for RNA transport by SID-1. J. Biol. Chem. *290*, 18904–18913.

Manche, L., Green, S.R., Schmedt, C., and Mathews, M.B. (1992). Interactions between double-stranded RNA regulators and the protein kinase DAI. Mol. Cell. Biol. *12*, 5238–5248.

Moser, A.R., Pitot, H.C., and Dove, W.F. (1990). A dominant mutation that predisposes to multiple intestinal neoplasia in the mouse. Science *247*, 322–324.

Nguyen, T.A., Smith, B.R.C., Tate, M.D., Belz, G.T., Barrios, M.H., Elgass, K.D., Weisman, A.S., Baker, P.J., Preston, S.P., Whitehead, L., et al. (2017). SIDT2 transports extracellular dsRNA into the cytoplasm for innate immune recognition. Immunity *47*, 498–509.e6.

Orvedahl, A., MacPherson, S., Sumpter, R., Tallóczy, Z., Zou, Z., and Levine, B. (2010). Autophagy protects against Sindbis virus infection of the central nervous system. Cell Host Microbe *7*, 115–127.

Osman, F., Jarrous, N., Ben-Asouli, Y., and Kaempfer, R. (1999). A cis-acting element in the 3′-untranslated region of human TNF-alpha mRNA renders splicing dependent on the activation of protein kinase PKR. Genes Dev. *13*, 3280–3293.

Pataer, A., Raso, M.G., Correa, A.M., Behrens, C., Tsuta, K., Solis, L., Fang, B., Roth, J.A., Wistuba, I.I., and Swisher, S.G. (2010). Prognostic significance of RNA-dependent protein kinase on non-small cell lung cancer patients. Clin. Cancer Res. *16*, 5522–5528.

Peisley, A., Jo, M.H., Lin, C., Wu, B., Orme-Johnson, M., Walz, T., Hohng, S., and Hur, S. (2012). Kinetic mechanism for viral dsRNA length discrimination by MDA5 filaments. Proc. Natl. Acad. Sci. U S A *109*, E3340–E3349.

Peisley, A., Lin, C., Wu, B., Orme-Johnson, M., Liu, M., Walz, T., and Hur, S. (2011). Cooperative assembly and dynamic disassembly of MDA5 filaments for viral dsRNA recognition. Proc. Natl. Acad. Sci. U S A *108*, 21010–21015.

Puthenveetil, S., Whitby, L., Ren, J., Kelnar, K., Krebs, J.F., and Beal, P.A. (2006). Controlling activation of the RNA-dependent protein kinase by siRNAs using site-specific chemical modification. Nucleic Acids Res. *34*, 4900–4911.

Schonborn, J., Oberstraβ, J., Breyel, E., Tittgen, J., Schumacher, J., and Lukacs, N. (1991). Monoclonal antibodies to double-stranded RNA as probes of RNA structure in crude nucleic acid extracts. Nucleic Acids Res. *19*, 2993–3000.

Shih, J.D., and Hunter, C.P. (2011). SID-1 is a dsRNA-selective dsRNA-gated channel. RNA *17*, 1057–1065.

Sledz, C.A., Holko, M., de Veer, M.J., Silverman, R.H., and Williams, B.R.G. (2003). Activation of the interferon system by short-interfering RNAs. Nat. Cell Biol. *5*, 834–839.

Su, L.K., Kinzler, K.W., Vogelstein, B., Preisinger, A.C., Moser, A.R., Luongo, C., Gould, K.A., and Dove, W.F. (1992). Multiple intestinal neoplasia caused by a mutation in the murine homolog of the APC gene. Science *256*, 668–670.

Taghavi, N., and Samuel, C.E. (2012). Protein kinase PKR catalytic activity is required for the PKR-dependent activation of mitogen-activated protein kinases and amplification of interferon beta induction following virus infection. Virology *427*, 208–216.

Uhlen, M., Zhang, C., Lee, S., Sjöstedt, E., Fagerberg, L., Bidkhori, G., Benfeitas, R., Arif, M., Liu, Z., Edfors, F., et al. (2017). A pathology atlas of the human cancer transcriptome. Science *357*, eaan2507.

Yoneyama, M., and Fujita, T. (2010). Recognition of viral nucleic acids in innate immunity. Rev. Med. Virol. *20*, 4–22.

Youssef, O.A., Safran, S.A., Nakamura, T., Nix, D.A., Hotamisligil, G.S., and Bass, B.L. (2015). Potential role for snoRNAs in PKR activation during metabolic stress. Proc. Natl. Acad. Sci. U S A *112*, 5023–5028.

Yu, C., Xiong, Q., Zhang, Y., and Wang, L. (2015). Lysosomal integral membrane protein Sidt2 plays a vital role in insulin secretion. Int. J. Clin. Exp. Pathol. *8*, 15622–15631.

iScience, Volume *20*

Supplemental Information

SIDT2 RNA Transporter Promotes Lung and Gastrointestinal Tumor Development

Tan A. Nguyen, Kathryn T. Bieging-Rolett, Tracy L. Putoczki, Ian P. Wicks, Laura D. Attardi, and Ken C. Pang

Supplemental Figure 1

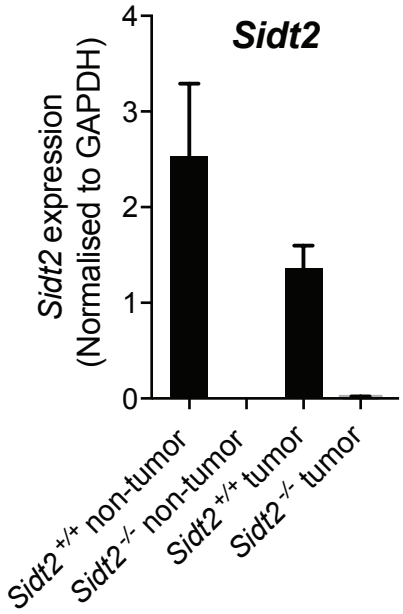

Supplemental Figure 1 – *Sidt2* is expressed in normal intestinal and tumour tissue in the distal small intestine of *Apc*$^{min/+}$ mice. Related to Figure 2.
Sidt2 expression in tumour and adjacent non-tumour tissue isolated from 100-day old *Sidt2*$^{+/+}$;*Apc*$^{min/+}$ and *Sidt2*$^{-/-}$;*Apc*$^{min/+}$ mice assessed via qRT-PCR. n = 5 mice per group. Data is plotted as mean ± SEM.

Supplemental Figure 2

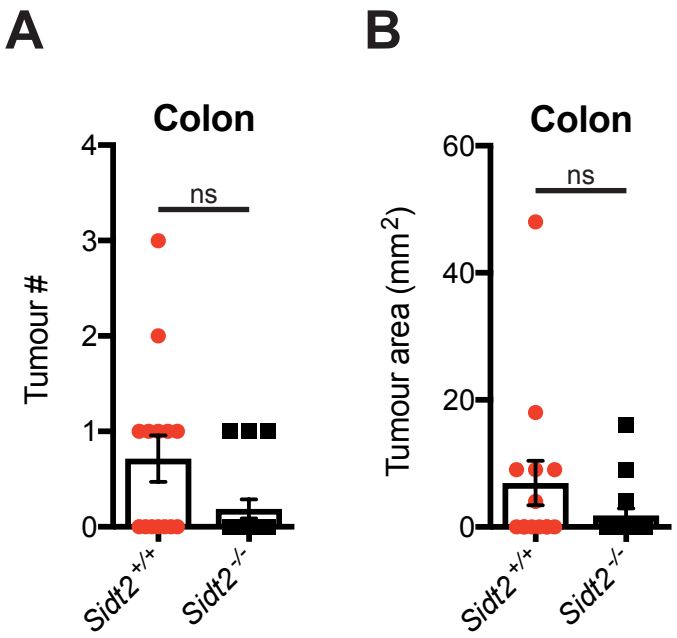

Supplemental Figure 2 – Loss of SIDT2 does not affect tumor burden in *Apc*$^{min/+}$ mouse model. Related to Figure 2.

Total number **(A)** and area **(B)** of visible tumors in the colon and small intestine (distal, medial and proximal) was quantified in 100-day old *Apc*$^{min/+}$;*Sidt2*$^{+/+}$ (n=12) and *Apc*$^{min/+}$;*Sidt2*$^{-/-}$ (n=12) mice. Error bars represent ± SEM.

Supplemental Figure 3

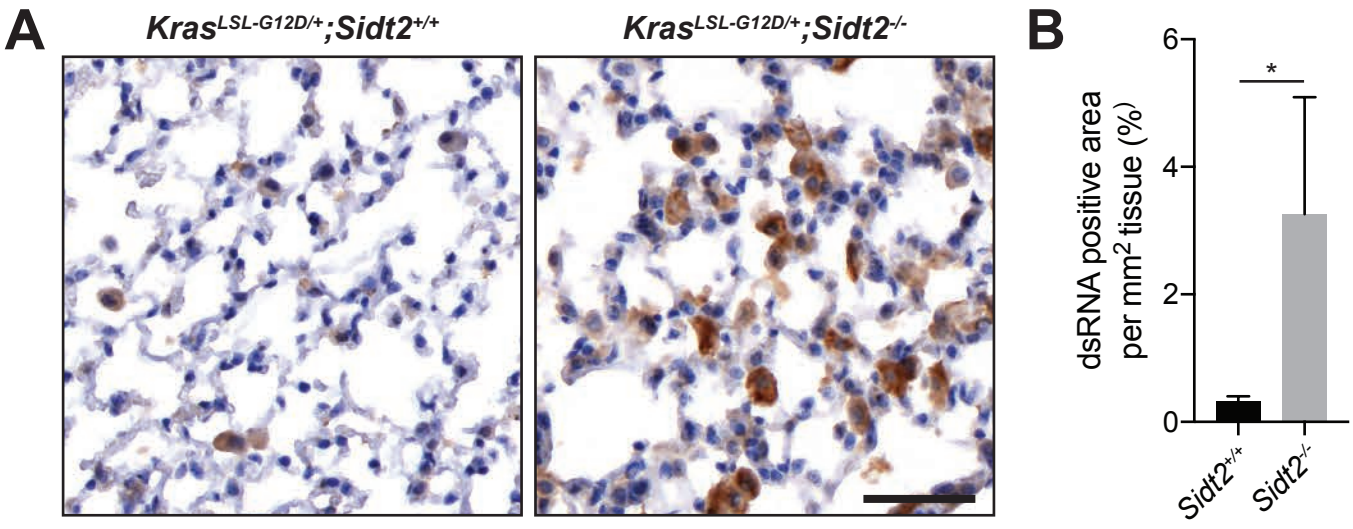

Supplemental Figure 3 – Loss of SIDT2 leads to accumulation of cytosolic dsRNA in the lungs of *Kras*$^{LSL\text{-}G12D/+}$; *Sidt2*$^{-/-}$ mice. Related to Figure 4.

(A) Representative image of dsRNA staining of lung sections from *Kras*$^{LSL\text{-}G12D/+}$; *Sidt2*$^{+/+}$ and *Kras*$^{LSL\text{-}G12D/+}$; *Sidt2*$^{-/-}$ mice. **(B)** Quantification of dsRNA-positive stained area per non-tumour area (n = 6 mice per genotype). Error bars represent ± SEM. * indicates $P < 0.05$ as calculated by Mann Whitney non-parametric test.

Supplemental Figure 4

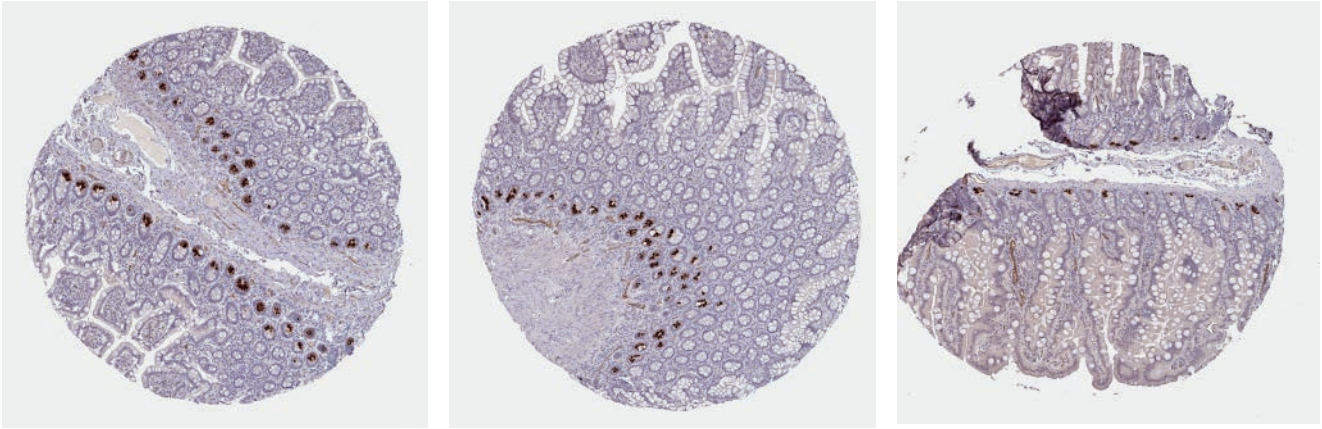

Supplemental Figure 4 – Human SIDT2 is expressed in glandular crypts of small intestine. Related to Figure 4 and Figure 5.

Publicly accessible images from The Human Protein Atlas of immunohistochemical stained sections of human small intestine from 3 individual healthy patient samples shows strong cytoplasmic localisation of SIDT2 in glandular cells (Uhlen et al., 2017).

Supplemental Figure 5

A

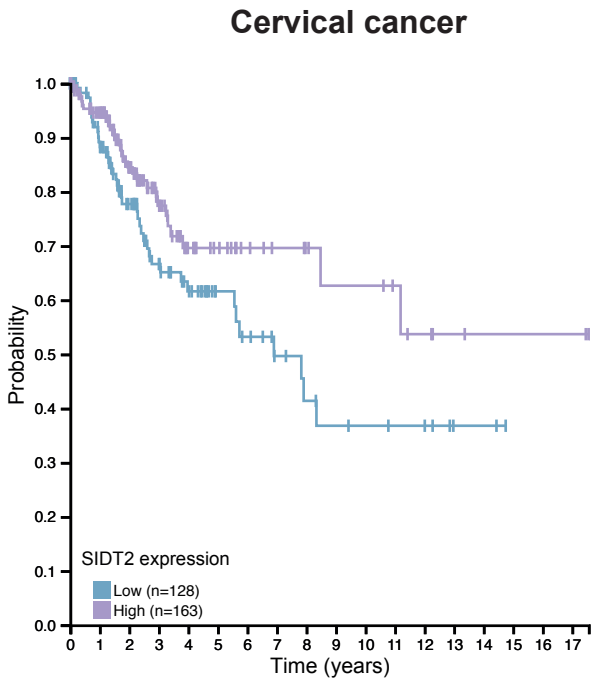

B

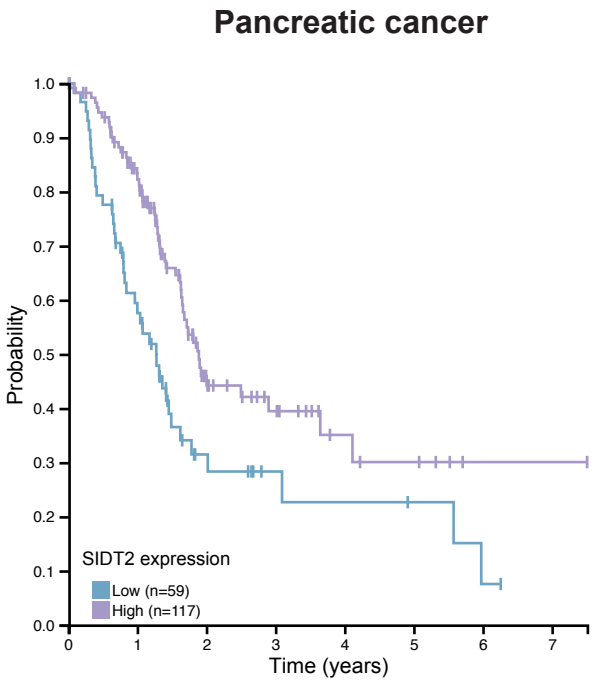

Supplemental Figure 5 – Lower SIDT2 expression is associated with lower survival for pancreatic and cervical cancer. Related to Figure 6.

Kaplan–Meier curves of overall survival of **(A)** cervical and **(B)** pancreatic cancer patients stratified against *SIDT2* expression from publicly available RNAseq data. The results shown are based upon data generated by the TCGA Research Network: http://cancergenome.nih.gov/.

TRANSPARENT METHODS

Mice

Mice were bred and maintained in the animal facilities at the Walter and Eliza Hall Institute of Medical Research (WEHI) and at the Department of Radiation Oncology, Stanford University, according to national and institutional guidelines for animal care. Mice were housed in individual ventilated cages at 19 - 24 ºC and maintained on a 14 h light to 10 h dark cycle with continuous access to Barastoc Custom Mixed Ration (irradiated) and acidified and filtered water. Female and male mice were used in experiments and were pooled for analysis. All experimental procedures were approved by the relevant animal ethics committees at the WEHI and Stanford University.

Analysis of *Kras$^{LSL\text{-}G12D/+}$* LUAD mouse model

Kras$^{LSL\text{-}G12D/+}$;*Sidt2$^{-/-}$* and *Kras$^{LSL\text{-}G12D/+}$*;*Sidt2$^{+/+}$* aged 6-8 weeks were inoculated with 4x10^6 PFU Adenovirus containing Cre recombinase (University of Iowa Viral Vector Core) by intra-tracheal intubation(DuPage et al., 2009). Eighteen weeks after inoculation, the lungs were harvested, fixed in 10% formalin, and bread-loafed into approximately 12 pieces per lung. The pieces were sectioned, stained with hematoxylin and eosin (H&E) as described below, and analyzed for tumor number and tumor burden.

Histological analyses

For histological examination of the intestine, colon, distal, medial and proximal portions of the small intestine were slit open longitudinally and the intraluminal contents removed. Each segment was then rolled up from the distal end to the proximal end using a “Swiss-rolling” technique (Williams et al., 2016). Preparations were then fixed in 10% (w/v) neutral-buffered formalin for at least 12 hours before embedding in paraffin, sectioned (3 μm), and prepared for general staining and immunohistochemistry (IHC). For frozen sections, Swiss roll preparations

were frozen and embedded in Optimal Cutting Temperature (OCT) using a PrestoCHILL system (Milestone), and sectioned (10 μm) for immunofluorescence staining. For H&E staining, slides were incubated with hematoxylin to stain nuclei (5 min), washed in dH_2O (1 min), incubated in 0.3% (v/v) acid ethanol to de-stain (1 dip), rinsed in dH_2O followed by Scott's tap water, then incubated in eosin (1 min). Slides were then rinsed in dH_20, dehydrated, cleared and mounted.

Immunohistochemistry and TUNEL staining

Automated staining was performed using the Dako Omnis EnVision G2 template. Dewax was performed with Clearify Clearing Agent (Dako) for 15 minutes, and antigen retrieval was done with EnVision FLEX TRS, High pH (Dako) at 97ºC for 30 minutes. Antibody against Ki67 (Cell Signaling #9129) and cleaved Caspase-3 (Asp175) (R&D Systems) was diluted 1:100 in EnVision Flex Antibody Diluent (Dako) and incubated at 32°C 60 minutes. Envision+ System-HRP Labelled Polymer Anti-Rabbit antibodies (Dako) were incubated for 20 min at 32ºC. Slides were counter-stained with Mayer Hematoxylin, dehydrated, cleared, and mounted with MM24 Mounting Medium (Surgipath-Leica). Tissue sections were imaged using the 3D Histech Slide Scanner and quantification analysis of Ki67 and cleaved caspase 3 positive cells was performed using ImageJ. For TUNEL staining, slides were prepared and stained using ApopTag® Red In Situ Apoptosis Detection Kit (Merk Millipore) according to manufacturer's instructions and imaged on a Zeiss Axio Observer wide-field fluorescence microscope.

Immunofluorescence staining of dsRNA

Frozen sections were fixed in 4% paraformaldehyde for 10 min on ice and washed 3 times in cold PBS permeabilized using 0.1% Tween/PBS, blocked in 5% normal goat serum for 1 h and stained with J2 (SciCon) primary antibody (1:200) overnight. Slides were subsequently washed 3 times for 5 min in PBS and then incubated with anti-mouse Alexa-594 secondary antibody for 1 h at room temperature. Sections were washed 3 times for 5 min in PBS and then cover-

slipped and mounted using Fluoroshield mounting medium with DAPI (Sigma Aldrich). Stained sections were imaged on a Zeiss Axio Observer wide-field fluorescence microscope.

Western blotting

Intestinal tumor and adjacent non-tumor tissue were lysed in KALB lysis buffer supplemented with protease inhibitor and phosphatase inhibitor (Roche) and then homogenized using a QIAGEN TissueLyser II, according to manufacturer's instructions. Homogenates were subsequently cleared by centrifugation at 13,000 rpm at 4°C for 20 minutes and denatured in 4x SDS PAGE sample buffer at 95°C for 5 min. 60µg of protein lysate was separated on NUPAGE Novex 4-12% Bis-Tris Gels (Life Technologies), and transferred electrophoretically to PVDF membranes, blocked in 5% BSA/TBST, incubated with the relevant primary antibodies overnight. Membranes were incubated for 1 h with horseradish peroxidase-conjugated secondary antibodies, washed, treated with Luminata Forte Western HRP substrate (Millipore), and visualized on the ChemiDoc MP system (Bio-Rad). Primary antibodies used were: total eiF2α (Cell Signaling, #9722, 1:1000), phospho-eIF2α (Cell Signaling, # 9721, 1:1000), phospho-JNK (Cell Signaling, #4668P, 1:1000), total JNK (Cell Signaling, #9252, 1:1000), pro-caspase 8 (WEHI in-house antibody, 1:1000), mouse specific cleaved caspase-8 (Asp387) (Cell Signaling #9429, 1:1000), Hsp70 (Thermo Fisher Scientific, #MA3-007, 1:10 000).

Analysis of *SIDT2* expression on cancer patient survival

Maximally separated Kaplan–Meier curves of overall survival of cancer patients stratified against *SIDT2* expression were generated from data by the TCGA Research Network: http://cancergenome.nih.gov/ and accessed via The Human Protein Atlas (Uhlen et al., 2017). Based on the FPKM value of SIDT2, patients were classified into two expression groups and the correlation between expression level and patient survival was examined.

Statistical analysis

Statistical analyses were performed in GraphPad Prism 7 software using unpaired, two-tailed student's t-tests, except in the case of the survival analysis, where a generalized Wilcoxon (Gehan–Breslow) test was used to compare survival curves. *P* values < 0.05 were considered statistically significant.

SUPPLEMENTAL REFERENCES

DuPage, M., Dooley, A.L., Jacks, T., 2009. Conditional mouse lung cancer models using adenoviral or lentiviral delivery of Cre recombinase. Nat Protoc 4, 1064–1072. doi:10.1038/nprot.2009.95

Uhlen, M., Zhang, C., Lee, S., Sjöstedt, E., Fagerberg, L., Bidkhori, G., Benfeitas, R., Arif, M., Liu, Z., Edfors, F., Sanli, K., Feilitzen, von, K., Oksvold, P., Lundberg, E., Hober, S., Nilsson, P., Mattsson, J., Schwenk, J.M., Brunnström, H., Glimelius, B., Sjöblom, T., Edqvist, P.-H., Djureinovic, D., Micke, P., Lindskog, C., Mardinoglu, A., Ponten, F., 2017. A pathology atlas of the human cancer transcriptome. Science 357, eaan2507. doi:10.1126/science.aan2507

Williams, J.M., Duckworth, C.A., Vowell, K., Burkitt, M.D., Pritchard, D.M., 2016. Intestinal Preparation Techniques for Histological Analysis in the Mouse. Curr Protoc Mouse Biol 6, 148–168. doi:10.1002/cpmo.2